International Journal of Pharmaceutics 436 (2012) 840–850

Contents lists available at SciVerse ScienceDirect

International Journal of Pharmaceutics

journal homepage: www.elsevier.com/locate/ijpharm

Pharmaceutical Nanotechnology

Penetratin-functionalized PEG–PLA nanoparticles for brain drug delivery

Huimin Xia[a,1], Xiaoling Gao[b,1], Guangzhi Gu[a], Zhongyang Liu[a], Quanyin Hu[a], Yifan Tu[a], Qingxiang Song[b], Lei Yao[b], Zhiqing Pang[a], Xinguo Jiang[a], Jun Chen[a,*], Hongzhuan Chen[b,**]

[a] Key Laboratory of Smart Drug Delivery, Ministry of Education & PLA, School of Pharmacy, Fudan University, Lane 826, Zhangheng Road, Shanghai 201203, PR China
[b] Department of Pharmacology, Institute of Medical Sciences, Shanghai Jiaotong University School of Medicine, 280 South Chongqing Road, Shanghai 200025, PR China

ARTICLE INFO

Article history:
Received 1 June 2012
Received in revised form 3 July 2012
Accepted 17 July 2012
Available online 24 July 2012

Keywords:
Blood–brain barrier (BBB)
Nanoparticles
Brain targeting
Cell-penetrating peptides
Penetratin

ABSTRACT

Nanoparticulate drug delivery system possesses distinct advantages for brain drug delivery. However, its amount that reach the brain is still not satisfied. Cell-penetrating peptides (CPPs), short peptides that facilitate cellular uptake of various molecular cargo, would be appropriate candidates for facilitating brain delivery of nanoparticles. However, such effect could be deprived by the rapid systemic clearance of CPPs-functionalized nanoparticles due to their positive surface charge. Penetratin (CPP with relatively low content of basic amino acids) was here functionalized to poly(ethylene glycol)–poly(lactic acid) nanoparticles (NP) to achieve desirable pharmacokinetic and biodistribution profiles for brain drug delivery. The obtained penetratin-NP showed a particle size of 100 nm and zeta potential of −4.42 mV. The surface conjugation of penetratin was confirmed by surface chemical compositions analysis via X-ray photo electron spectroscopy. In MDCK–MDR cell model, penetratin-NP presented enhanced cellular accumulation via both lipid raft-mediated endocytosis and direct translocation processes with the involvement of Golgi apparatus, lysosome and microtubules. In vivo pharmacokinetic and biodistribution studies showed that penetratin-NP exhibited a significantly enhanced brain uptake and reduced accumulation in the non-target tissues compared with low-molecular-weight protamine (CPP with high arginine content)-functionalized nanoparticles. These data strongly implicated that penetratin-NP might represent a promising brain-targeting drug delivery system. The findings also provided an important basis for the optimization of brain drug delivery systems via surface charge modulation.

1. Introduction

Central nervous system (CNS) diseases represent the largest and fastest growing area of unmet medical need. However, drug delivery into the brain is made difficult by the presence of the blood–brain barrier (BBB), which is formed by tight junctions within the capillary endothelium of the vertebrate brain (Abbott et al., 2006; Pardridge, 1999, 2005). Efflux transporters such as P-glycoprotein (P-gp) and other multidrug resistance-associated proteins (MRP) isoforms that located at the BBB also play an important role in hindering the passage of drugs into the CNS (Dallas et al., 2006; Kusuhara and Sugiyama, 2001). Nanoparticulate drug delivery system possesses distinct advantages for brain drug delivery (Ojewole et al., 2008; Yang, 2010). However, the amount of the nanoparticles that can reach the brain is still not satisfied (Hu et al., 2009; Lu et al., 2005). An important strategy utilized for improving the brain delivery of nanoparticles is their surface modification with ligands that with binding moieties or receptors expressed at the luminal surface of cerebral endothelial cells, allowing drug trafficking across the BBB via adsorptive-mediated transcytosis (AMT) or receptor-mediated transcytosis (RMT) (Hu et al., 2009; Lu et al., 2005; Yang, 2010).

CNS delivery via adsorptive transcytosis is triggered by electrostatic interactions between the positively charged moieties on the nanoparticles and negatively charged membrane surface regions on the brain endothelial cells (Herve et al., 2008; Lu et al., 2005). Considering a relative high concentration of negative charges exists at the BBB, positively charged nanoparticles would create a selective environment for AMT-mediated brain delivery. However, positively charged particles often exhibit a rapid blood clearance together with a high accumulation in the lung and liver (Li and Huang, 2008). Therefore, in order to achieve a desirable pharmacokinetic and biodistribution profiles for enhancing CNS drug delivery, it of high importance to carefully control the surface charge of the delivery systems.

Cell-penetrating peptides (CPPs), often contain protein transduction domains (PTDs), are peptides of 5–40 amino acids in length

* Corresponding author. Tel.: +86 21 51980066; fax: +86 21 51980069.
** Corresponding author. Tel.: +86 21 63846590/776451.
E-mail addresses: chenjun@fudan.edu.cn (J. Chen), hongzhuan_chen@hotmail.com (H. Chen).
[1] These authors contributed equally to this work.

0378-5173/$ – see front matter © 2012 Elsevier B.V. All rights reserved.
http://dx.doi.org/10.1016/j.ijpharm.2012.07.029

with the ability to gain access to the cell interior and across complex physiological barriers (Liu et al., 2008; Rao et al., 2008; Zorko and Langel, 2005). More than 100 CPPs have been identified, the common feature is that they are amphipathic and net positively charged (Zorko and Langel, 2005). Due to their positive charge, CPPs would be appropriate candidates for facilitating brain drug delivery at least partly via the AMT mechanism. However, their capability to deliver therapeutics through the BBB has been rarely reported, excepted the most-studied CPP – TAT (Liu et al., 2008; Rao et al., 2008; Suk et al., 2006). In our previous work, low-molecular-weight protamine (LMWP, CVSRRRRRRGGRRRR, the proportion of basic amino acids is 66.7%), a CPP with similar sequence with TAT, was functionalized to the surface of poly(ethylene glycol)–poly(lactic acid) (PEG–PLA) nanoparticles (LMWP-NP). A significantly enhanced nose-to-brain drug delivery of LMWP-NP was achieved following intranasal administration (Xia et al., 2011). However, a less effective brain delivery efficiency was obtained after intravenous administration. Considering that positively charged particles tend to form aggregates in the presence of negatively charged serum proteins and result in enhanced accumulation in the lung and liver (Li and Huang, 2008), we speculated that the poor brain delivery efficiency of LMWP-NP following intravenous administration could be resulted from the high arginine content of LMWP. Therefore, we proposed that if a less positive charged CPP chosen for NP functionalization, a more desirable pharmacokinetic and biodistribution profile and effective brain delivery would be achieved.

Penetratin, also known as pAntp peptide, is a peptide sequence from Drosophila Antennapedia homeodomain (amino acids 43–58, RQIKIWFQNRRMKWKK, the proportion of basic amino acids is 43.75%, lower than that of LMWP) (Magzoub et al., 2002). It has been reported that penetratin crossed the BBB within 10 min at a level of 0.9%ID/g (the percentage of injected dose per gram of tissue) in the brain and its permeability was 2–3-fold higher than that of the most frequently used TAT and SynB 1 (Sarko et al., 2010). Therefore, penetratin might be practically employed as an attractive CPP for facilitating brain drug delivery.

In the present study, penetratin was functionalized to PEG–PLA nanoparticles aiming at obtaining CPPs-NP with better pharmacokinetic property for brain delivery. Using coumarin-6 as the fluorescence probe, cellular uptake of penetratin-NP as well as the mechanism of cellular internalization was investigated in the MDCK–MDR cell model. In order to evaluate the effect of surface charge modulation on the brain delivery efficiency of nanoparticles, pharmacokinetic and biodistribution profiles of penetratin-NP were quantitatively determined and compared with that of unmodified NP and LMWP-NP.

2. Materials and methods

2.1. Materials and animals

The copolymers of methoxy poly(ethylene glycol)$_{3000}$–poly(lactic acid)$_{34,000}$ (MePEG–PLA) and maleimide –poly(ethylene glycol)$_{3400}$–poly(lactic acid)$_{34,000}$ (Male–PEG–PLA) were kindly provided by East China University of Science and Technology. Penetratin (CRQIKIWFQNRRMKWKK) was synthesized by ChinaPeptides Co. Ltd. (Shanghai, China). Coumarin-6, coumarin-7 and 1,1′-dioctadecyl-3,3,3′,3′-tetramethyl indotricarbocyanine Iodide (DiR) were obtained from Sigma–Aldrich (St. Louis, MO, USA). 4,6-Diamidino-2-phenylindole (DAPI) was provided by Molecular Probes (Eugene, OR, USA), and cell counting kit-8 (CCK-8) by Dojindo Laboratories (Japan). Dulbecco's Modified Eagle Medium (DMEM) (high glucose) cell culture medium and fetal bovine serum (FBS) were both purchased from Gibco (Carlsbad, CA, USA). Penicillin/streptomycin stock solutions and 0.25% Trypsin–EDTA were provided by Invitrogen Co., USA. Plastic cell culture dishes, plates and flasks were obtained from Corning Incorporation (Lowell, MA, USA). All the other materials were of analytical reagent grades and used without further purification.

Adult male nude mice (16–20 g), ICR mice (18–22 g, ♀) and Sprague-Dawley rats (180–220 g, ♀) were obtained from Experimental Animal Center of Fudan University and maintained at 22 ± 2 °C on a 12 h light–dark cycle with access to food and water ad libitum. The animals used for experiment were treated according to the protocols approved by the ethical committee of Fudan University.

2.2. Preparation of penetratin-functionalized nanoparticle

PEG–PLA nanoparticles loaded with coumarin-6 were prepared using an emulsion/solvent evaporation technique (Gao et al., 2006; Tobio et al., 1998). In brief, 1 mL of dichloromethane solution containing MePEG–PLA (22.5 mg), Male–PEG–PLA (2.5 mg) and coumarin-6 (25 μg) was added into 2 mL of 1% sodium cholate solution, and the mixture was emulsified by sonication (280 w, 2.4 min) on ice using a probe sonicator (Ningbo Scientz Biotechnology Co. Ltd., China). The O/W emulsion was diluted into an 8 mL of 0.5% sodium cholate aqueous solution under rapid magnetic stirring for 5 min. After evaporating the organic phase at 30 °C with a ZX-98 rotavapor (Shanghai Institute of Organic Chemistry, China), the nanoparticles were obtained by centrifugation at 14,000 rpm for 45 min using TJ-25 centrifuge (Beckman Counter, USA). The supernatant was discarded, and the nanoparticles were reconstituted in double-distilled water and subjected to a 1.5 cm × 20 cm sepharose CL-4B column (Pharmacia Biotech Inc., Sweden) for removing the unentrapped coumarin-6.

Nanoparticles modified with penetratin (penetratin-NP) were prepared via a maleimide-thiol coupling reaction at room temperature for 8 h as described previously (Gao et al., 2006). The products were then eluted with 0.01 M HEPES buffer (pH 7.0) through the 1.5 cm × 20 cm sepharose CL-4B column to remove the unconjugated peptide.

2.3. Characterization of penetratin-NP

Particle size and zeta potential of the nanoparticles were determined by dynamic light scattering (DLS) using a Nicomp™ 380 XLS Zeta Potential/Particle Sizer (PSS·Nicomp, USA). A transmission electron microscope (TEM, H-600, Hitachi, Japan) was used for the morphological examination.

To verify the surface modification with penetratin, the nanoparticles samples were lyophilized using an ALPHA 2-4 Freeze Dryer (0.070 Mbar Vakuum, −80 °C, Martin Christ, Germany) and subjected to XPS analysis. Data analysis was carried out with the RBD AugerScan 3.21 software provided by RBD Enterprises.

2.4. In vitro release of coumarin-6

In vitro release of coumarin-6 from the nanoparticles was determined under different pH conditions to evaluate if the fluorescence tracer remained associated with the particles during a 24 h incubation period. NP and penetratin-NP were incubated at 37 °C in pH 4 and pH 7.4 PBS at the coumarin-6 concentration of 50 ng/mL under the shaking rate of 100 rpm. In order to omit the influence of time-related quenching of the fluorescence, the cumulative release percentage (CR%) of coumarin-6 from nanoparticles was determined as described below. Half of the periodic samples (0 min, 5 min, 15 min, 30 min, 1 h, 2 h, 4 h, 8 h, 12 h, 24 h) (n = 3) were subject to centrifugation at 14,000 rpm for 45 min with the supernatant diluted with methanol and analyzed to determine the amount of

the released coumarin-6, while the left half of the parallel samples ($n = 3$) were simultaneously determined to show the total coumarin-6 amount retained in the samples at each time point (the samples were vortexed with three-fold volumes of acetonitrile and diluted to a proper concentration for determination). A 20 μL diluted sample was injected in the HPLC system (Shimadzu Scientific Instrument Inc., Japan) consisted of a pump (LC-10ATVP) and a fluorescence detector (Model RF-10AXL, Ex 465 nm/Em 502 nm). With a Dikma Diamonsil C18 (5 μm, 200 mm × 4.6 mm) column, the separations were achieved with methanol:water (96:4) mobile phase at the flow rate at 1.2 mL/min and column temperature at 35 °C. The cumulative release percentage (CR %) of coumarin-6 from nanoparticles at the individual time points was calculated using the following equation:

$$CR\ (\%) = \frac{\text{amount of coumarin-6 in the supernatant}}{\text{total amount of coumarin-6}} \times 100$$

2.5. Cell experiments

2.5.1. Cell culture

MDCK–MDR cells, stemmed from Madin-Darby canine kidney (MDCK), with overexpression of multidrug resistance proteins (MDR), were maintained in Dulbecco's Modified Eagle Medium supplemented with 10% FBS, penicillin (100 U/mL) and streptomycin (100 mg/mL) under standardized conditions (95% relative humidity, 5% CO_2, 37 °C).

2.5.2. Qualitative fluorescent microscopy analysis of cellular association of penetratin-NP

MDCK–MDR cells were seeded in a 96-well plate at the density of 5×10^3 cells/well. Twenty-four hours later, the cells were incubated with coumarin-6-loaded NP and penetratin-NP solution in HBSS (containing coumarin-6 25–300 ng/mL) at 37 °C for 2 h, respectively. At the end of the experiment, the cells were washed three times with PBS and fixed with 3.7% formaldehyde for 10 min. After that, the cells were washed three times with PBS, and observed under a fluorescence microscope (Olympus, Japan).

2.5.3. Quantitative HCS analysis of cellular uptake of penetratin-NP

MDCK–MDR cells were seeded in a 96-well plate at the density of 5×10^3 cells/well. Twenty-four hours later, the medium was replaced with the nanoparticles solution (10–600 μg/mL) and incubated for 1 h at 4 °C and 37 °C, respectively. After that, the cells were washed with PBS, fixed in a 3.7% formaldehyde solution for 10 min, and stained with 10 μg/mL Hochest 33258 at room temperature, away from light for 10 min. After washing with PBS for three times, the cells were subjected to detection under a KineticScan® HCS Reader (Version 3.1, Cellomics Inc., Pittsburgh, PA, USA) (Gao et al., 2008). For determining the fluorescent signals from the internalized nanoparticles, the cells were incubated with trypan blue (Beyotime Institute of Biotechnology) to quench those fluorescent signals from the uninternalized nanoparticles, and subjected to a second reading (Scott and Woods, 2000).

In a separate experiment, to characterize the effects of incubation time on nanoparticle uptake, the cells were incubated with 100 μL of nanoparticles solution (100 μg/mL) for 30 min, 1, 2 and 4 h at 37 °C, respectively, and the quantitative analysis was performed as described above.

In order to reveal the mechanism of cellular uptake of penetratin-NP in MDCK–MDR cells, cellular association of the nanoparticles were determined in the presence of various endocytosis inhibitors. The cells were preincubated for 30 min with 5 μg/mL filipin, 4 μg/mL colchicines, 5 μg/mL BFA, 200 nM monensin, 20 μM nocodazole, and 2.5 mM methyl-β-cyclodextrin (M-β-CD), respectively, and then incubated with 90 μg/mL of NP or penetratin-NP at 37 °C for 1 h. After that, quantitative analysis was performed as described above.

2.5.4. Cytotoxicity of penetratin-NP

One hundred microliters of MDCK–MDR cells were seeded in a 96-well plate at the density of 5×10^3 cells/well and incubated at 37 °C with 5% CO_2 for 24 h to allow cell attachment. After that, the cells were subjected to NP and penetratin-NP treatment at the different concentrations from 0.01 to 2.0 mg/mL for 3 h. Cells without exposure to the NP samples were used as control. Cell viability was evaluated by CCK-8 method via calculating the percentage of absorbance of sample groups in comparison with that of the control (Gao et al., 2011).

2.6. In vivo imaging analysis of biodistribution of penetratin-NP

In order to study the brain distribution profile of penetratin-NP and compared it with that of NP, coumarin-6-labeled NP and penetratin-NP were given to SD rats ($n = 3$) via tail vein injection. Each animal received a total amount of nanoparticles at 0.5 mg (containing 20 μg of coumarin-6, in 0.5 mL). One hour following administration, the animals were anesthetized with 10% hydral, heart perfused with 100 mL of saline and 200 mL of 4% paraformaldehyde sequentially for fixation. After that, the brains were removed, further fixed in 4% paraformaldehyde for 24 h, dehydrated with sucrose solution, and subjected to OCT (Sakura, Torrance, CA, USA) embedding and frozen section. Finally, the sections were transferred to microscope slides, counterstained with DAPI (100 ng/mL) and observed under a fluorescence microscope (Olympus IX71).

To study the body distribution profiles of NP and penetratin-NP, near infrared dye DiR was employed as the fluorescent probe. The DiR-loaded NP or penetratin-NP was prepared using the method described above. Under anesthesia, nude mice (DiR 0.5 mg/kg, $n = 3$) was intravenously injected with the nanoparticle formulations via the tail vein. Fluorescent image of each animal was captured at selected time points post administration. In a separate experiment, ICR mice were periodic sacrificed with the brains harvested and subjected to imaging under a Maestro in vivo imaging system (CRI, MA).

2.7. Pharmacokinetic and biodistribution analysis

In vivo pharmacokinetics of penetratin-NP after vein injection were evaluated in Sprague-Dawley rats and compared with that of NP and LMWP-NP. Fifteen rats were randomly divided into three groups, and injected with coumarin-6-loaded NP, penetratin-NP and LMWP-NP, respectively, at the coumarin-6 dose of 0.8 mg/kg. At the time points (0.083, 0.5, 1, 2, 4, 8 and 12 h) after administration, blood was collected into the tube with heparin and stored at −20 °C until analysis.

For biodistribution analysis, seventy-two ICR mice were divided into three groups, dosed with the unconjugated NP, penetratin-NP and LMWP-NP, respectively. Each animal intravenously received a total of 0.25 mL nanoparticles (containing 20 μg of coumarin-6). At each time points (0.08, 0.17, 0.5, 1, 2, 4, 8 and 12 h) following the administration, the animals were euthanized with blood collected into a tube with heparin and brains, hearts, livers, spleens, lungs, and kidneys harvested and stored until analysis.

Blood concentrations of coumarin-6 were determined by reverse-phase high performance liquid chromatography coupled with tandem mass spectrometry (LC–MS/MS) detection. Briefly, 100 μL of blood and 10 μL of internal standard (coumarin-7, 10 ng/mL) were extracted twice with 1.0 mL of *n*-hexane. The total organic layer was separated by centrifugation at 6000 rpm

for 10 min, and transferred to a clean tube. The drug residue was obtained by evaporation under a stream of nitrogen at 40 °C and reconstituted in a methanol–water (50:50, v/v) solution. After centrifugation at 12,000 rpm for 10 min, 5 μL aliquots of the supernatant were injected into the LC–MS/MS system for analysis. Tissue samples were homogenized with 3-fold volumes of saline. The homogenate (about 0.2 mL) was mixed with 10 μL of internal standard (coumarin-7, 10 ng/mL) and extracted with 1.0 mL of *n*-hexane twice. The drug residues were obtained as described above and reconstituted in 100 μL of a solution containing methanol–water (50:50, v/v). Aliquots of 5 μL were injected into the LC–MS/MS system for analysis. The API 3000 triple quadrupole LC–MS/MS system (Applied Biosystems, Toronto, Canada) was equipped with electrospray ionization (ESI) source, a G1312A quaternary pump, a G1379A vacuum degasser, a G1316A thermostatted column oven (Agilent, Waldbronn, Germany) and an HTS PAL autosampler (CTC Analytics, Switzerland). A Venusil XBP Phenyl column (100 mm × 2.1 mm, 5 μm, Agela, Shanghai, China) with a mobile phase of methanol–2 mM ammonium acetate–formic acid (90:10:0.1, v/v/v) was used for chromatographic separations. The flow rate and column temperature were set at 0.3 mL/min and 40 °C, respectively. Quantitation was achieved with MS–MS detection in positive ion mode for both the analyte and IS. The ion spray voltage was set at 5000 V. Source temperature was maintained at 500 °C. Nitrogen was used as the nebulizing gas (8 L/min) and curtain gas (8 L/min). For collision activated dissociation (CAD), nitrogen was employed as the collision gas at a pressure of 4 L/min. The compound parameters, such as declustering potential (DP), collision energy (CE), entrance potential (EP) and collision cell exit potential (CXP) were 100, 50, 10, 15 V for coumarin-6, 80, 50, 10, 15 V for IS respectively. Detection of the ions was performed in the multiple-reaction monitoring (MRM) mode, by monitoring the transition pairs of *m*/*z* 351.3 precursor ion to the *m*/*z* 307.1 for coumarin-6, *m*/*z* 334.1 precursor ion to the *m*/*z* 290.1 for coumarin-7. Quadrupoles Q1 and Q3 were set on unit resolution. Data acquisition was performed with Analyst 1.4.1 software package (Applied Biosystems). The results were plotted as ng/mL blood–time curve in the blood and ng/g tissue–time curves in brain as well as other tissues from 0.08 to 12 h.

The pharmacokinetic data analysis was performed by means of a model independent method. The terminal elimination rate constant (k) was determined by least-square regression analysis of terminal log-linear portions of the plasma concentration–time profile ($k = -2.303 \times$ slope). The elimination half-life ($t_{1/2}$) was calculated as $0.693/k$. The area under the curve to the last measurable concentration (AUC_{0-t}) was calculated by the linear trapezoidal rule. The clearance (CL) was calculated as X_0/AUC. Biodistribution data analysis was performed using Drug and Statistics software for Windows (DAS ver 2.1.1, China). Targeting efficiency (TE), relative uptake efficiency (RE) and concentration efficiency (CE) were calculated to evaluate the brain targeting efficiency of the NPs (Chen et al., 2009).

2.8. Statistical analysis

All the data were expressed as mean ± standard deviation. Comparison between multiple groups was carried out by one-way ANOVA followed by Bonferroni tests. Statistical significance was defined as $p < 0.05$.

3. Results

3.1. Characterization of penetratin-NP

The nanoparticles, prepared from a blend of MePEG–PLA and Male–PEG–PLA with the emulsion/solvent evaporation method, exhibited a volume-based diameters of around 90 nm, and increased to around 100 nm after penetratin conjugation. The polydispersity of all the formulations showed quite narrow size distribution (Fig. 1A). Representative transmission electron

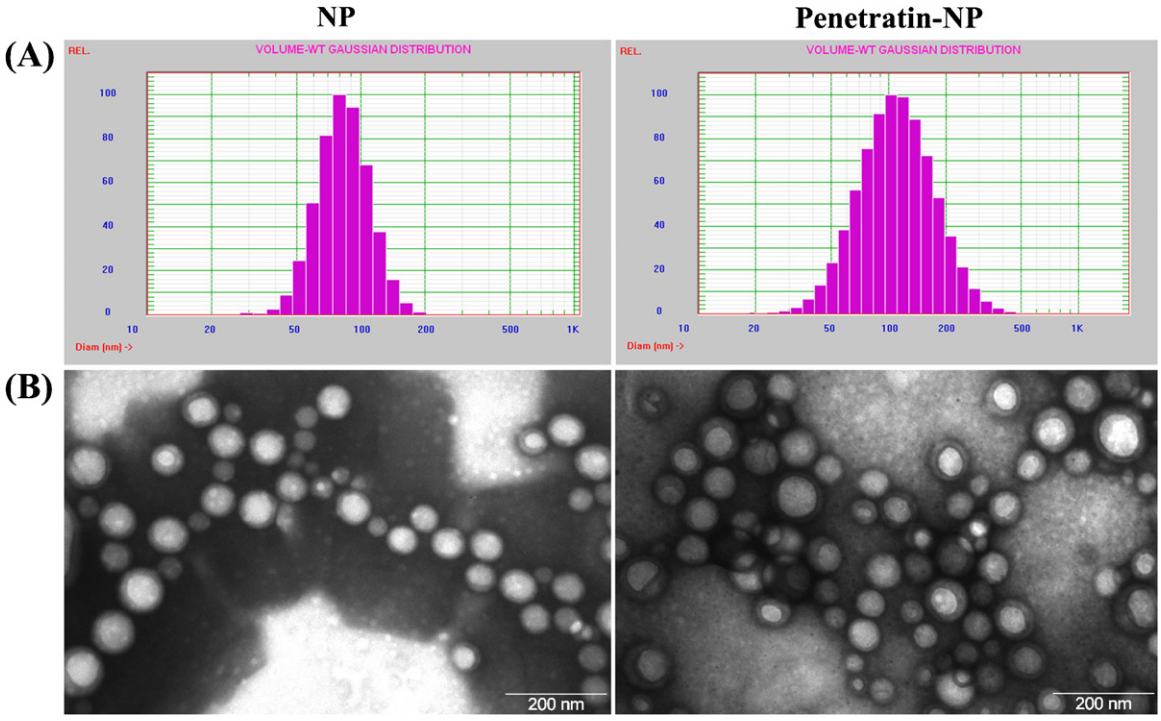

Fig. 1. (A) Volume-based diameters and (B) transmission electron micrographs of NP and penetratin-NP.

Table 1
The surface elemental composition of NP and penetratin-NP.

Samples	XPS elemental ratio (%)			XPS C1s envelope ratio (%)				XPS O1s envelope ratio (%)	
	C	O	N	C—C/C—H	C—O—C	C—O—C=O	O—C=O	O=C	O—C
				Binding energy (eV)					
				285.0	286.8	287.6	289.4	532.0	533.3
NP	64.2	35.8	–	41.0	24.5	20.5	14.0	45.9	54.1
Penetratin-NP	61.7	37.6	0.7	38.0	28.2	21.8	12.0	36.5	63.5

–, not detected.

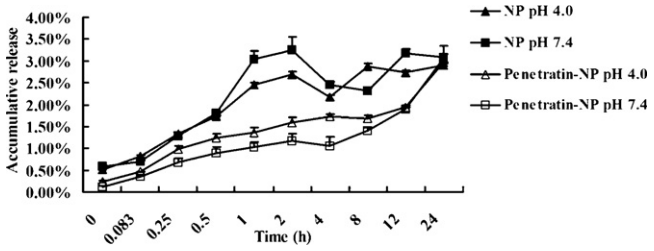

Fig. 2. In vitro release of coumarin-6 from NP and penetratin-NP in 0.1 M PBS buffer at pH 7.4 and 4.0, respectively.

micrographs (Fig. 1B) illustrated that NP and penetratin-NP were generally spherical with a uniform distribution.

Zeta potential of the NP formulations was about −20.5 mV, while that of penetratin-NP was −4.42 mV. The surface chemical compositions of NP and penetratin-NP were determined via XPS analysis (Table 1). The C1s spectra were composed of four peaks at 285.0, 286.8, 287.6 and 289.4 eV, respectively, and the peak at 286.8 eV mainly represented —C—O—C groups of the PEG component on the nanoparticle surface. The decomposition of the O1s envelope revealed the presence of two types of oxygen: O=C at 532.0 eV and O—C at 533.3 eV. The peak at 404 eV was attributed to Nitrogen N1s envelope and was only detected in penetratin-NP at a value of 0.7% with regard to the total amount of C, O, and N atoms.

3.2. In vitro release of coumarin-6

In vitro release study conducted at 37 °C in pH 4.0 and pH 7.4 PBS, which represented the pH of the endo-lysosomal compartment and physiologic pH respectively, showed that no more than 3.5% of coumarin-6 was released from NP and penetratin-NP after a 24 h incubation period (Fig. 2).

3.3. Qualitative fluorescent microscopy analysis of cellular association of penetratin-NP

Fluorescent microscopy analysis showed that following 2 h exposure to penetratin-NP and NP, the cellular associated fluorescent signals in MDCK cells correlated with the increase of nanoparticle concentration (Fig. 3). Apparently higher accumulation of the fluorescent signals was observed in those cells treated with penetratin-NP.

3.4. Quantitative HCS analysis of cellular uptake of penetratin-NP

Quantitative analysis showed the same concentration-dependant cellular uptake profile. The uptake of penetratin-NP was 4.59 times higher than that of NP at 300 μg/mL at 37 °C after 1 h incubation (Fig. 4A). Besides, the uptake of NP and penetratin-NP in MDCK–MDR cells was also temperature (Fig. 4A) and time dependent (Fig. 4B). At each time point, the uptake of penetratin-NP was higher than that of NP (about 2 times higher than that of NP after incubation for 1 h) (Fig. 4B).

Endocytosis inhibition experiments showed that M-β-CD inhibited both the cellular association of NP and penetratin-NP, while BFA, monensin, nocodazole and colchicines only presented inhibitory effect on the internalization of penetratin-NP (Fig. 5).

3.5. Cytotoxicity of penetratin-NP

CCK-8 method was used to evaluate the cytotoxicity of penetratin-NP. As shown in Fig. 6, the cell viability following NP and penetratin-NP treatments was both over 80% with no significant difference observed between the treatments.

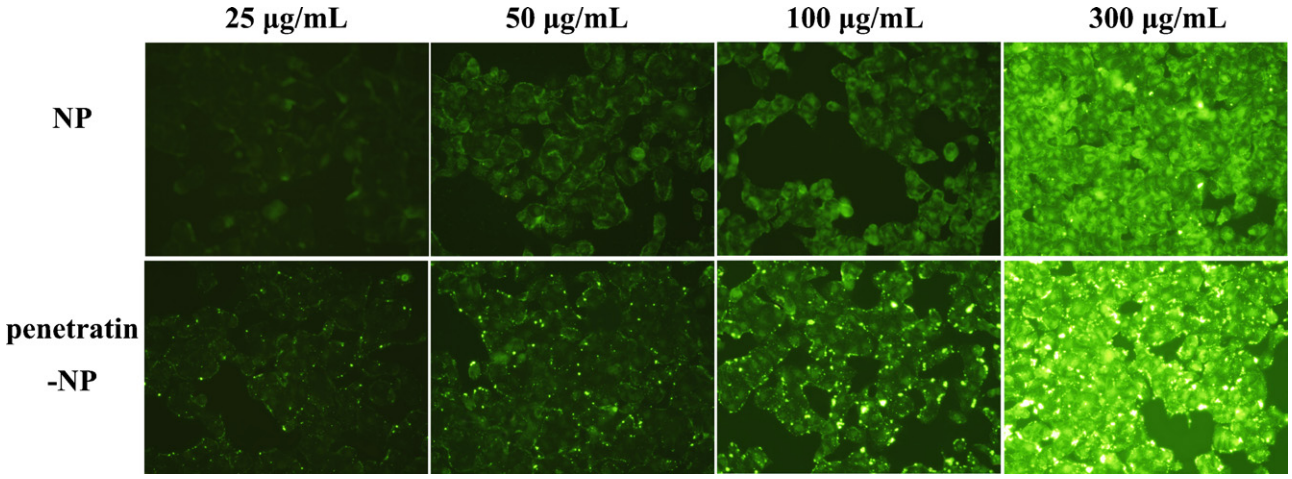

Fig. 3. In vitro cellular association of NP and penetratin-NP after 2 h incubation at 37 °C at the coumarin-6 concentrations of 25 ng/mL, 50 ng/mL, 100 ng/mL, 300 ng/mL, respectively.

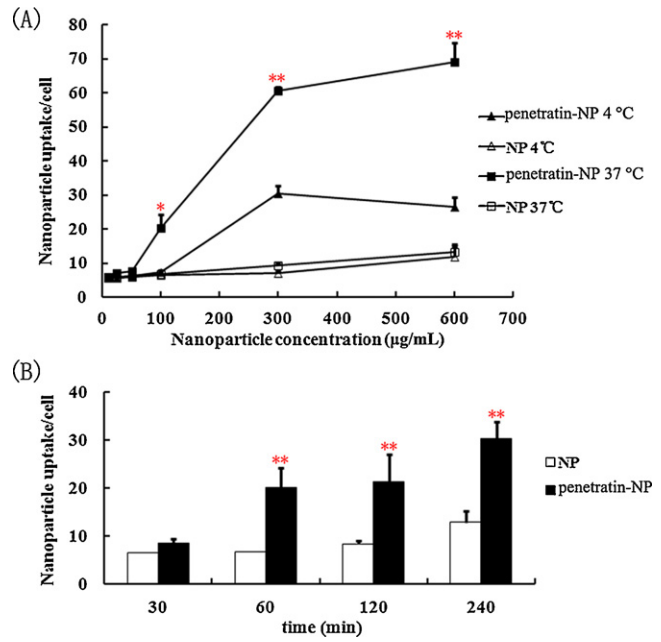

Fig. 4. Cellular uptake of NP and penetratin-NP in MDCK–MDR cells. (A) After 1 h incubation with 10–600 μg/mL of penetratin-NP and NP at 37 °C and 4 °C, respectively. (B) After the incubation with 100 μg/mL of penetratin-NP and NP at 37 °C for 30, 60, 120 and 240 min, respectively. $^{*}p < 0.05$, $^{**}p < 0.01$ significantly different from that of NP at the same temperature, same concentration and incubation time.

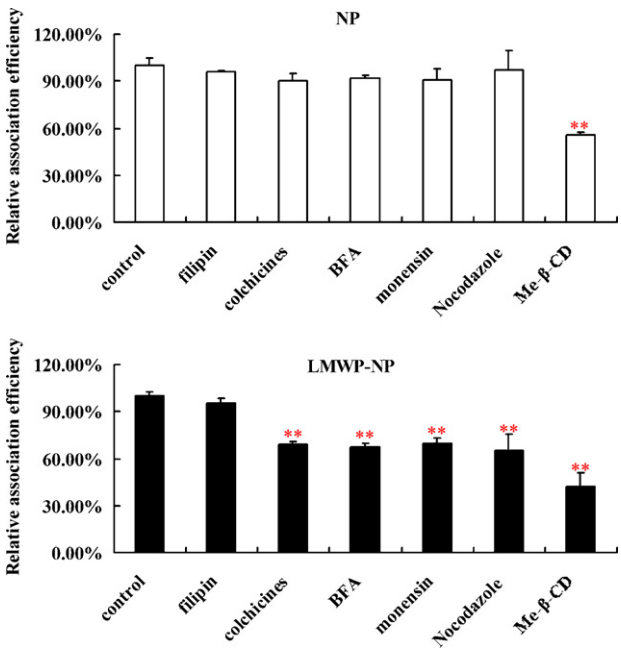

Fig. 5. Cellular association of NP and penetratin-NP in MDCK–MDR cells in the presence of different endocytosis inhibitors. Data represented mean ± SD, $n = 3$. $^{*}p < 0.05$, $^{**}p < 0.01$ significantly different from that of the non-inhibitor control.

3.6. In vivo imaging of the biodistribution of penetratin-NP

Fluorescence microscopy examination revealed that coumarin-6 signals was observed in the animal cortex, hippocampi, ventricle, thalamencephalon and sagittal raphe following intravenous injection of both NP and penetratin-NP. And the fluorescence signal observed in those rats treated with penetratin-NP was much higher than that in the NP-treated ones (Fig. 7).

For in vivo imaging, an obvious stronger fluorescence of DiR signal was detected in the brains of those animals administered with DiR-loaded penetratin-NP compared with that in those treated with DiR-loaded NP (Fig. 8).

3.7. Pharmacokinetic and biodistribution

Pharmacokinetics of penetratin-NP after vein injection were evaluated in SD rats and compared with that of NP and LMWP-NP. It was showed that NP and penetratin-NP have similar blood concentration–time curves (Fig. 9 and Table 2). In contrast, LMWP-NP showed a quicker systemic clearance and lower AUC_{0-t} (Fig. 9 and Table 2).

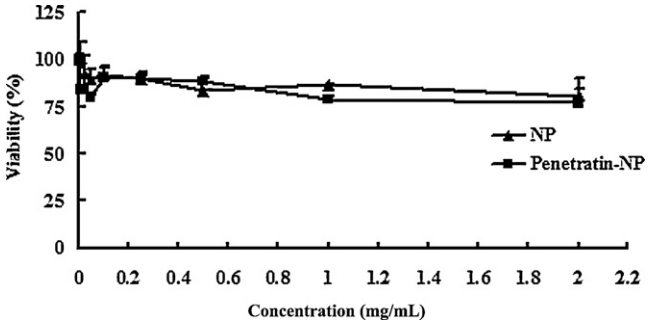

Fig. 6. In vitro cytotoxicity of NP and penetratin-NP on MDCK–MDR cells following a 3-h treatment at the nanoparticles concentrations ranging from 0 to 2 mg/mL, $n = 3$.

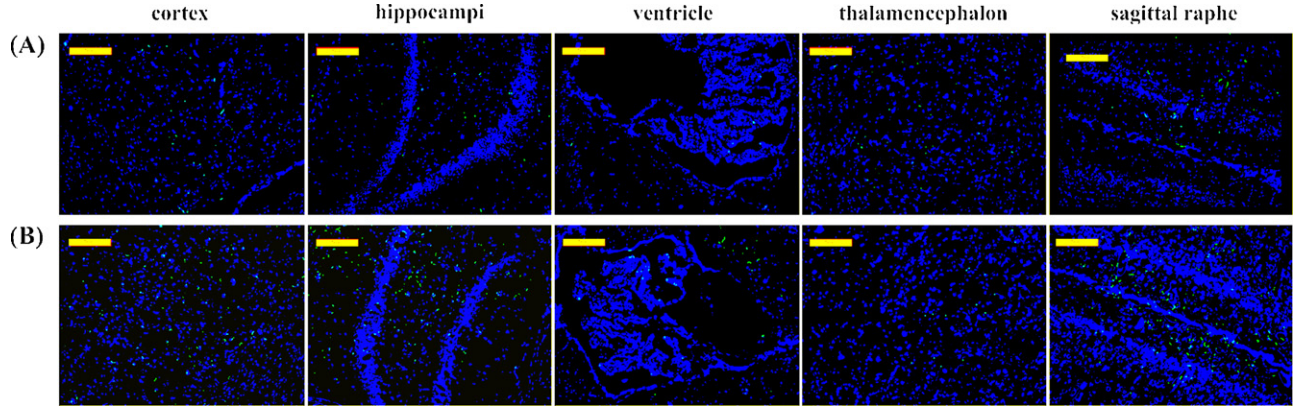

Fig. 7. Brain distribution of NPs in rats 1 h after intravenous administration of coumarin-6-loaded NP (A) and penetratin-NP (B), respectively. Green: coumarin-6-loaded nanoparticles; blue: cell nuclei stained with DAPI. Bar, 100 μm. (For interpretation of the references to color in this figure legend, the reader is referred to the web version of the article.)

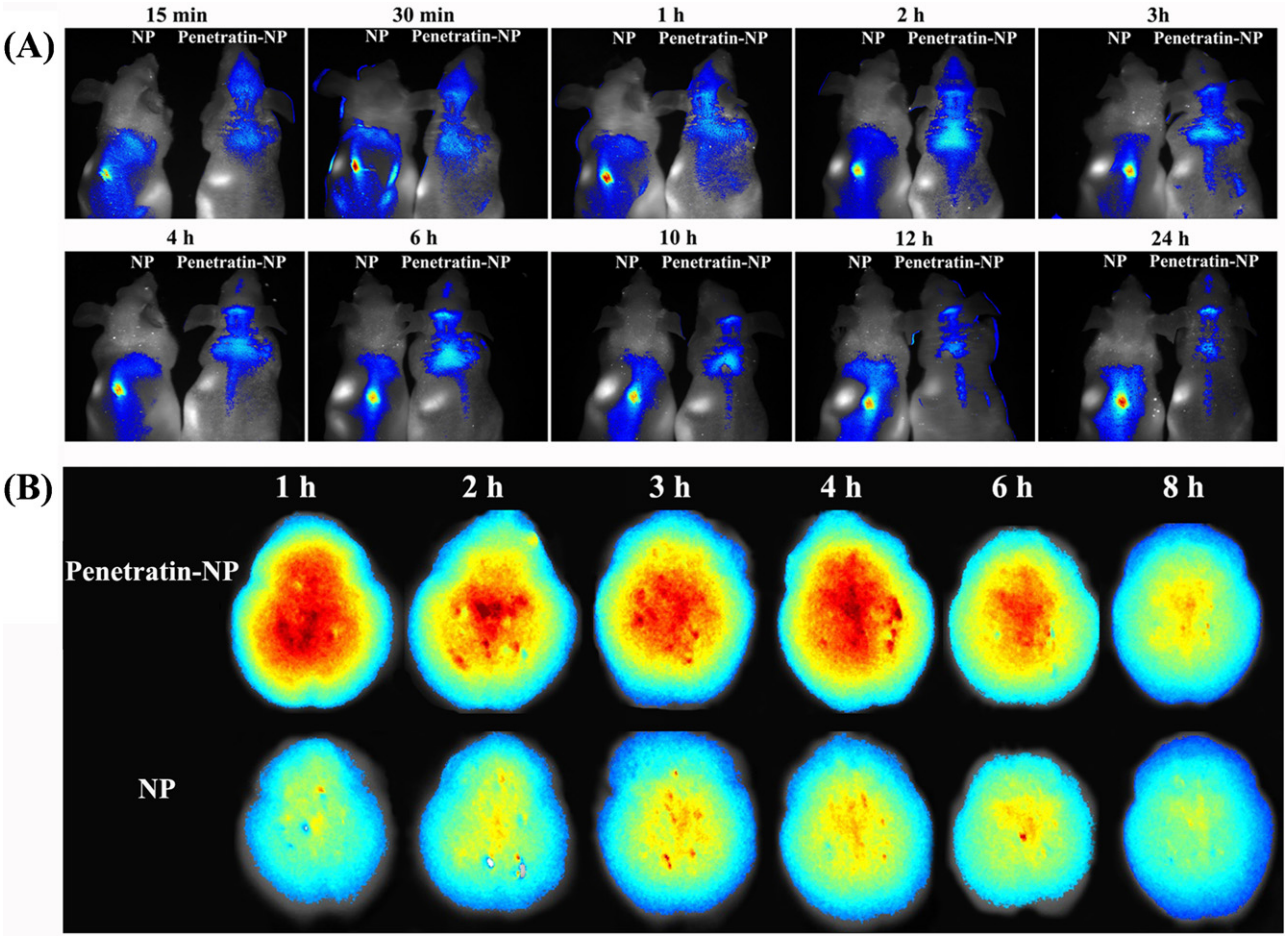

Fig. 8. In vivo distribution of DiR-loaded penetratin-NP and NP at various time points following intravenous administration. Representative optical images taken under a dedicated imaging system designed for small animals imaging. (A) Living nude mice and (B) the brains of ICR mice.

Table 2
Pharmacokinetic parameters of coumarin-6 after an intravenous administration of coumarin-6-loaded NP, penetratin-NP and LMWP-NP, respectively, to SD rats at the dose of 0.8 mg/kg.

Formulation	AUC_{0-t} (h ng/mL)	k (h^{-1})	$T_{1/2}$ (h)	CL (mL/h)
NP	207.22 ± 72.22	0.25 ± 0.04	2.83 ± 0.50	108.91 ± 44.73
Penetratin-NP	165.68 ± 32.84	0.26 ± 0.03	2.73 ± 0.35	124.30 ± 22.85
LMWP-NP	112.05 ± 19.76*	0.44 ± 0.02**,##	1.58 ± 0.09**,##	183.04 ± 32.76*,#

* $p < 0.05$, significant different with that of NP.
** $p < 0.01$, significant different with that of NP.
\# $p < 0.05$, significant different with that of penetratin-NP.
\#\# $p < 0.01$, significant different with that of penetratin-NP.

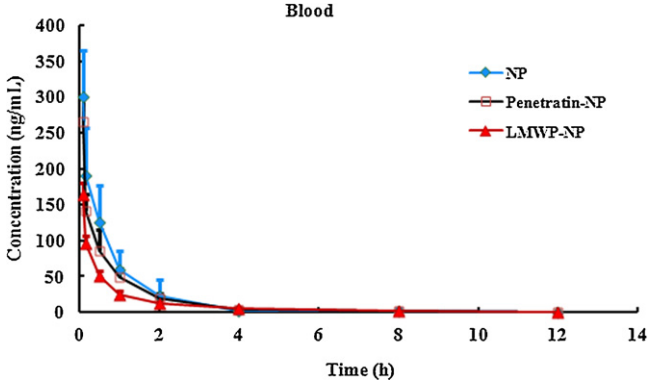

Fig. 9. Blood concentration–time profiles of coumarin-6 following intravenous administration of coumarin-6 loaded NP, penetratin-NP and LMWP-NP. Data represented the mean ± SD. $n = 5$.

Biodistribution of coumarin-6-loaded NP, penetratin-NP and LMWP-NP in ICR mice were quantitatively evaluated at various time points after injection (Fig. 10) with TE, RE and CE calculated to evaluate the brain targeting efficiency of the NPs (Table 3). A preferential localization of penetratin-NP in the brain was detected when compared with the unmodified NP and LMWP-functionalized NP. The AUC_{0-t} of coumarin-6 in the brain following the penetratin-NP treatment was 1.89-fold compared with that after NP injection, while that after LMWP-NP treatment was only 1.26-fold. The C_{max} of penetratin-NP was 2.59-fold compared with that of NP while that of LMWP-NP was 1.39-fold. Biodistribution of coumarin-6 in the various tissues is shown in Fig. 10, which showed that the NPs mainly accumulated in liver and lung, and the amount of LMWP-NP in the spleen, liver, and lung was significantly higher than that of NP and penetratin-NP (especially at the earlier time points).

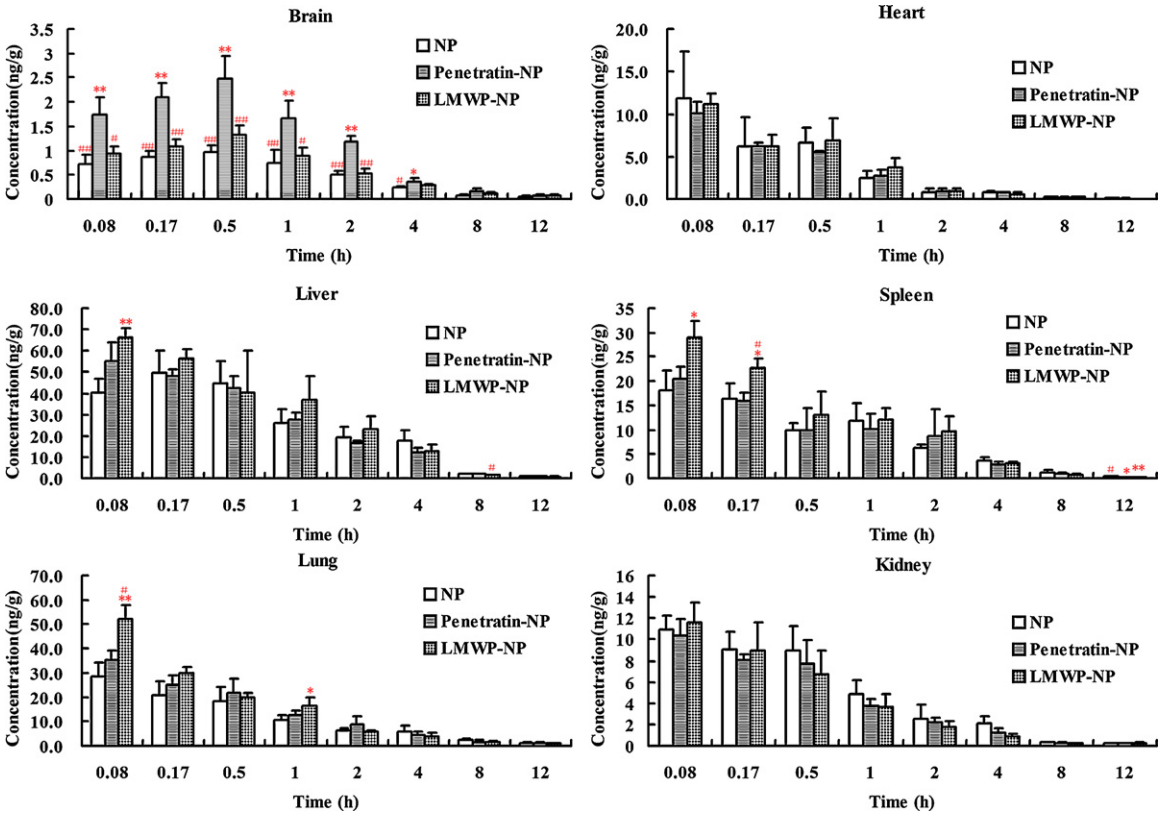

Fig. 10. Biodistribution of coumarin-6 following intravenous administration of coumarin-6-loaded NP, penetratin-NP and LMWP-NP, respectively. $n = 3$. $^{*}p < 0.05$, $^{**}p < 0.01$, statistical significance with functionalized nanoparticles (penetratin-NP, LMWP-NP) versus NP; $^{\#}p < 0.05$, $^{\#\#}p < 0.01$, statistical significance with LMWP-NP and NP versus penetratin-NP.

4. Discussion

Endothelial tight junctions together with the efflux transporters at the BBB greatly limits the distribution of therapeutics into the central nervous system (CNS). Positively charged CPPs-functionalized nanoparticles have been proposed as promising DDS for improving brain-targeted delivery at least partly via adsorptive-mediated transcytosis. However, the brain delivery efficiency of the CPPs-functionalized nanoparticles could be deprived by their rapid systemic clearance due to their positive surface charge. In order to optimize CPPs-functionalized nanoparticles for brain drug delivery, penetratin (CPP with relatively low content of basic amino acids) was here functionalized to PEG–PLA nanoparticles with pharmacokinetic and biodistribution profiles characterized and compared with that of low-molecular-weight protamine (CPP with high arginine content)-funtionalized nanoparticles.

Despite the vast number of biomaterials eligible for nanoparticles preparation, only a few of them are suitable for brain delivery. The complexity of the CNS calls for biomaterials that are non-toxic, fully biodegradable and well-characterized. Biodegradable polymers, poly(lactic acid) (PLA), fit these criteria. It has been used for the development of nanoparticulate drug delivery systems to deliver a variety of therapeutic compounds and showed favorable safety profiles (Gao et al., 2006; Lu et al., 2005). Poly(ethylene glycol) (PEG) was chosen to reduce systemic clearance of nanoparticles (Alexis et al., 2008; Calvo et al., 2001; Olivier et al., 2002). In addition, the functionalization of PEG end groups with maleimide also made it possible to conjugate the targeting moiety – penetratin.

The nanoparticles were characterized by means of morphology, particle size, zeta potential and element analysis. Particle size is an important characteristic that associated with the endocytosis by brain capillary cells. Particles from 5 to 250 nm, in general, exhibit higher transport efficiency (Alexis et al., 2008). The nanoparticles obtained here with diameters of approximately 100 nm met such requirement. The zeta potential of the unmodified NP was negative (−20.5 mV), while that of penetratin-NP was relatively positive (−4.42 mV). The increase in zeta potential was very likely contributed by the net positively charged penetratin. Such evidence suggested the existence of penetratin on the surface of penetratin-NP, which was further justified by XPS analysis. According to the surface chemical composition of NP and penetratin-NP, the nitrogen signal was ascribed to the maleimide group of maleimide–PEG–PLA or penetratin. However, the nitrogen signal failed to be detected in the unfunctionalized NP, suggesting that the nitrogen contribution by the maleimide group can be neglected. Since XPS determines the elemental and average chemical composition of the material at its surface in 5–10 nm depth and the instrumental detection limit of XPS is 0.1% (Wagner et al., 2002), the N signal detected in the penetratin-NP sample was therefore believed to be attributed to penetratin on the nanoparticles surface.

The results of in vitro release that conducted in pH 4.0 and pH 7.4 PBS at 37 °C were consistent with that reported in previous studies (Gao et al., 2006; Hu et al., 2009; Lu et al., 2005), suggesting that coumarin-6 could be used as a fluorescent probe for evaluating both in vitro and in vivo behavior of the NPs.

In vitro cellular association of NP and penetratin-NP was determined in MDCK–MDR cells. MDCK–MDR cells, which form tighter junctions than Caco-2 cells (Wang et al., 2005), with a high expression of human-derived P-gp (about 25 times higher than that in MDCK cells) (Zhang and Benet, 1998) and similar physiological characteristics to BBB (Veronesi, 1996), are considered as an ideal cell model for evaluating the BBB permeability of CNS therapeutic candidates (Gumbleton and Audus, 2001; Wang et al., 2005).

Table 3
Pharmacokinetic parameters for biodistribution of coumarin-6 after an intravenous administration of coumarin-6-loaded NP, penetratin-NP and LMWP-NP, respectively, to ICR mice at the dose of 20 μg of coumarin-6.

Formulation	Tissue	C_{max} (ng/mL or g)	T_{max} (h)	AUC_{0-t} (h ng/mL or g)	TE	RE	CE
NP	Blood	301.20	0.08	232.05	–	–	–
	Brain	0.97	0.50	3.05##	–	–	–
	Heart	13.26	0.08	11.14	0.27	–	–
	Liver	54.84	0.17	125.23	0.02	–	–
	Spleen	19.36	0.08	38.58	0.08	–	–
	Lung	28.99	0.08	52.40	0.06	–	–
	Kidney	11.08	0.08	19.84	0.15	–	–
Penetratin-NP	Blood	265.00	0.08	188.37	–	–	–
	Brain	2.52	0.50	5.78**	–	1.89	2.59
	Heart	10.10	0.08	11.71	0.49	–	–
	Liver	55.25	0.08	126.71	0.05	–	–
	Spleen	20.62	0.08	43.85	0.13	–	–
	Lung	35.27	0.08	62.47	0.09	–	–
	Kidney	10.36	0.08	17.42	0.33	–	–
LMWP-NP	Blood	164.80	0.08	128.97*	–	–	–
	Brain	1.35	0.50	3.84#	–	1.26	1.39
	Heart	10.38	0.08	11.55	0.33	–	–
	Liver	67.87	0.08	126.22	0.03	–	–
	Spleen	28.02	0.08	44.98	0.09	–	–
	Lung	53.06	0.08	56.33	0.07	–	–
	Kidney	11.94	0.08	14.72	0.26	–	–

$TE = (AUC_{0-t})_T/(AUC_{0-t})_{NT}$; $RE = (AUC_{0-t})_f/(AUC_{0-t})_c$; $CE = (C_{max})_f/(C_{max})_c$ where T and NT represent target tissue (brain) and non-target tissue (heart, liver, spleen, lung, kidney), respectively; f and c represent functionalized nanoparticles (penetratin-NP, LMWP-NP) and control (NP), respectively.
* $p < 0.05$, significant different with that of NP.
** $p < 0.01$, significant different with that of NP.
\# $p < 0.05$, significant different with that of penetratin-NP.
\## $p < 0.01$, significant different with that of penetratin-NP.

As the fluorescent microscopy analysis showed, penetratin-NP exhibited an apparently higher cellular accumulation than unmodified NP, suggesting that penetratin conjugation on the surface of nanoparticles could facilitate their cellular uptake. A time-, temperature- and concentration-dependant cellular uptake of the nanoparticles was observed, suggesting a process of active endocytosis. To characterize the endocytosis pathways involved in the cellular uptake of penetratin-NP, cellular association experiments were performed in the presence of various endocytosis inhibitors, including the caveolae-mediated endocytosis pathway inhibitor – filipin (Mo and Lim, 2004), lipid raft inhibitor – M-β-CD (Vercauteren et al., 2010), Golgi apparatus destroyer – BFA (Jiang et al., 2006), lysosome inhibitor – monensin (Gabor et al., 2002) and microtubules depolymerization agent – nocodazole (Zegers et al., 1998) and colchicines (Abulrob et al., 2005). Both the cellular association of NP and penetratin-NP were inhibited by M-β-CD, suggesting the involvement of lipid raft-mediated endocytosis in the cellular uptake of both nanoparticles. Besides, BFA, monensin, nocodazole and colchicines also showed inhibitory effect on the internalization of penetratin-NP, suggesting that Golgi apparatus, lysosome and microtubules also involved in its cellular transport. In addition, cellular internalization of penetratin-NP was also observed at low temperature (4 °C) (Fig. 4A), although much lower than that at 37 °C, but still higher than that of NP at both 37 and 4 °C, suggesting that besides endocytosis, energy-independent internalization mechanism might also involve in the cellular internalization of penetratin-NP. We speculated it to be ascribed to the direct translocation effect of penetratin (Derossi et al., 1998; Fonseca et al., 2009; Futaki, 2002). Therefore, the mechanisms described so far should be shared between two general pathways: endocytosis and direct translocation.

The property of cationized proteins to efficiently penetrate cells raises the concern about its potential toxicity. CCK-8 method was here used to determine cell viability for evaluating the safety of penetratin-NP. Since PLA is generally accepted as a safe polymer with good biocompatibility and biodegradability, unconjugated PLA-NP was regarded as the safe control. No significant difference was observed following both the penetratin-NP and NP treatments, suggesting that penetratin-NP might be considered as a promising drug carrier without observable cytotoxic effects.

Qualitative fluorescence microscopy analysis showed that coumarin-6 signals was extensively observed in animal CNS (cortex, hippocampi, ventricle, thalamencephalon and sagittal raphe) following intravenous injection of penetratin-NP, suggesting its ability of delivery agents to a wide CNS area. In addition, the fluorescence signal observed in those animals treated with penetratin-NP was much higher of than that in NP-treated ones (Fig. 7). Quantitatively, a preferential brain accumulation of penetratin-NP was also observed over both the unmodified and LMWP-functionalized NP. Targeting efficiency (TE), relative uptake efficiency (RE) and concentration efficiency (CE) were calculated to evaluate the brain targeting efficiency of the NPs. $RE > 1$ was achieved by both penetratin-NP and LMWP-NP, indicating that both of them possessed the capability for brain delivery. The higher RE value obtained by penetratin-NP suggested its relative preferential brain-targeting efficiency over LMWP-NP. Besides, the higher CE value was obtained by the CPPs-NP especially by penetratin-NP, indicating its rapid and effective distribution into the CNS. Furthermore, much higher TE values was achieved by penetratin-NP, indicating its enhanced accumulation in the brain and relatively reduced distribution in the non-target organs.

In order to interpret the reason why penetratin-NP exhibited a relative superiority in brain delivery over both NP and LMWP-NP, in vivo pharmacokinetics of the NP formulations in both the circulation and the major organs were determined. Similar blood concentration–time profiles was obtained by both NP and penetratin-NP, suggesting that the conjugation of penetratin on the surface of NP did not impair the long-circulation characteristic of PEG (Table 2). In contrast, LMWP-NP showed a quicker systemic clearance and a significant reduction in AUC_{0-t}, which was speculated to be resulted from its rapid distribution to the non-target organs (Tables 2 and 3). Such hypothesis was verified by the

biodistribution analysis, which showed a higher accumulation of LMWP-NP in the spleen, liver, and lung, especially at the early time points (Fig. 10). In contrast, penetratin-NP exhibited a relative superiority in brain delivery efficiency. Penetratin-NP was found in brain within 15 min at the concentration 0.85-fold higher than LMWP-NP, which was speculated to be ascribed to its relative lower level of positive charge. As our previous studies showed (Xia et al., 2011), the zeta potential of LMWP-NP was about 2.42 mV, while that of penetratin-NP was only −4.42 mV. Positively charged nanoparticles tend to form aggregates in the presence of negatively charged serum proteins once i.v. administered and often exhibit a rapid blood clearance and a higher accumulation in the lung and liver (Zhang et al., 2005). Therefore, by comparing the in vivo biodistribution, we claimed that modification of nanoparticle system with CPPs with lower positively charge might contribute to higher brain delivery efficiency.

5. Conclusion

Penetratin (CPP with relatively low content of basic amino acids) was functionalized to PEG–PLA nanoparticles to achieve desirable pharmacokinetic and biodistribution profiles for brain drug delivery. The obtained penetratin-NP showed a particle size of 100 nm and zeta potential of −4.42 mV. The surface conjugation of penetratin was confirmed by X-ray photo electron spectroscopy analysis. In MDCK–MDR cell model, penetratin-NP presented enhanced cellular accumulation via both lipid raft-mediated endocytosis and direct translocation processes with the involvement of Golgi apparatus, lysosome and microtubules. In vivo pharmacokinetic and biodistribution studies showed that penetratin-NP exhibited a significantly enhanced brain uptake and reduced accumulation in the non-target organs compared with LMWP-NP. The data here implicated that penetratin-NP might serve as a promising brain-targeting delivery system for brain drug delivery. Our findings also provided an important basis for the optimization of brain-targeted drug delivery systems via surface charge modulation.

Acknowledgements

This work was supported by National Natural Science Foundation of China (81072592), National Key Basic Research Program (2010CB529800), National Science and Technology major Project (2012ZX09303001-001), Innovation Program of Shanghai Municipal Education Commission (12ZZ107), Program for New Century Excellent Talents in University and Grants from Shanghai Science and Technology Committee (10QA1404100, 11430702200).

References

Abbott, N.J., Ronnback, L., Hansson, E., 2006. Astrocyte-endothelial interactions at the blood-brain barrier. Nat. Rev. Neurosci. 7, 41–53.
Abulrob, A., Sprong, H., Van Bergen, E.H.P., Stanimirovic, D., 2005. The blood-brain barrier transmigrating single domain antibody: mechanisms of transport and antigenic epitopes in human brain endothelial cells. J. Neurochem. 95, 1201–1214.
Alexis, F., Pridgen, E., Molnar, L.K., Farokhzad, O.C., 2008. Factors affecting the clearance and biodistribution of polymeric nanoparticles. Mol. Pharm. 5, 505–515.
Calvo, P., Gouritin, B., Chacun, H., Desmaele, D., D'Angelo, J., Noel, J.P., Georgin, D., Fattal, E., Andreux, J.P., Couvreur, P., 2001. Long-circulating PEGylated polycyanoacrylate nanoparticles as new drug carrier for brain delivery. Pharm. Res. 18, 1157–1166.
Chen, Q., Gong, T., Liu, J., Wang, X., Fu, H., Zhang, Z., 2009. Synthesis, in vitro and in vivo characterization of glycosyl derivatives of ibuprofen as novel prodrugs for brain drug delivery. J. Drug Target. 17, 318–328.
Dallas, S., Miller, D.S., Bendayan, R., 2006. Multidrug resistance-associated proteins: expression and function in the central nervous system. Pharmacol. Rev. 58, 140–161.
Derossi, D., Chassaing, G., Prochiantz, A., 1998. Trojan peptides: the penetratin system for intracellular delivery. Trends Cell Biol. 8, 84–87.
Fonseca, S.B., Pereira, M.P., Kelley, S.O., 2009. Recent advances in the use of cell-penetrating peptides for medical and biological applications. Adv. Drug Deliv. Rev. 61, 953–964.
Futaki, S., 2002. Arginine-rich peptides: potential for intracellular delivery of macromolecules and the mystery of the translocation mechanisms. Int. J. Pharm. 245, 1–7.
Gabor, F., Schwarzbauer, A., Wirth, M., 2002. Lectin-mediated drug delivery: binding and uptake of BSA–WGA conjugates using the Caco-2 model. Int. J. Pharm. 237, 227–239.
Gao, X., Tao, W., Lu, W., Zhang, Q., Zhang, Y., Jiang, X., Fu, S., 2006. Lectin-conjugated PEG-PLA nanoparticles: preparation and brain delivery after intranasal administration. Biomaterials 27, 3482–3490.
Gao, X., Wang, T., Wu, B., Chen, J., Chen, J., Yue, Y., Dai, N., Chen, H., Jiang, X., 2008. Quantum dots for tracking cellular transport of lectin-functionalized nanoparticles. Biochem. Biophys. Res. Commun. 377, 35–40.
Gao, X., Yao, L., Song, Q., Zhu, L., Xia, Z., Xia, H., Jiang, X., Chen, J., Chen, H., 2011. The association of autophagy with polyethylenimine-induced cytotoxicity in nephritic and hepatic cell lines. Biomaterials 32, 8613–8625.
Gumbleton, M., Audus, K.L., 2001. Progress and limitations in the use of in vitro cell cultures to serve as a permeability screen for the blood–brain barrier. J. Pharm. Sci. 90, 1681–1698.
Herve, F., Ghinea, N., Scherrmann, J.M., 2008. CNS delivery via adsorptive transcytosis. AAPS J. 10, 455–472.
Hu, K., Li, J., Shen, Y., Lu, W., Gao, X., Zhang, Q., Jiang, X., 2009. Lactoferrin-conjugated PEG–PLA nanoparticles with improved brain delivery: in vitro and in vivo evaluations. J. Control. Release 134, 55–61.
Jiang, S., Rhee, S.W., Gleeson, P.A., Storrie, B., 2006. Capacity of the Golgi apparatus for cargo transport prior to complete assembly. Mol. Biol. Cell 17, 4105–4117.
Kusuhara, H., Sugiyama, Y., 2001. Efflux transport systems for drugs at the blood–brain barrier and blood-cerebrospinal fluid barrier (Part 1). Drug Discov. Today 6, 150–156.
Li, S.D., Huang, L., 2008. Pharmacokinetics and biodistribution of nanoparticles. Mol. Pharm. 5, 496–504.
Liu, L., Guo, K., Lu, J., Venkatraman, S.S., Luo, D., Ng, K.C., Ling, E.A., Moochhala, S., Yang, Y.Y., 2008. Biologically active core/shell nanoparticles self-assembled from cholesterol-terminated PEG–TAT for drug delivery across the blood–brain barrier. Biomaterials 29, 1509–1517.
Lu, W., Zhang, Y., Tan, Y.Z., Hu, K.L., Jiang, X.G., Fu, S.K., 2005. Cationic albumin-conjugated pegylated nanoparticles as novel drug carrier for brain delivery. J. Control. Release 107, 428–448.
Magzoub, M., Eriksson, L.E., Graslund, A., 2002. Conformational states of the cell-penetrating peptide penetratin when interacting with phospholipid vesicles: effects of surface charge and peptide concentration. Biochim. Biophys. Acta 1563, 53–63.
Mo, Y., Lim, L.Y., 2004. Mechanistic study of the uptake of wheat germ agglutinin-conjugated PLGA nanoparticles by A549 cells. J. Pharm. Sci. 93, 20–28.
Ojewole, E., Mackraj, I., Naidoo, P., Govender, T., 2008. Exploring the use of novel drug delivery systems for antiretroviral drugs. Eur. J. Pharm. Biopharm. 70, 697–710.
Olivier, J.C., Huertas, R., Lee, H.J., Calon, F., Pardridge, W.M., 2002. Synthesis of pegylated immunonanoparticles. Pharm. Res. 19, 1137–1143.
Pardridge, W.M., 1999. Blood–brain barrier biology and methodology. J. Neurovirol. 5, 556–569.
Pardridge, W.M., 2005. The blood–brain barrier: bottleneck in brain drug development. NeuroRx 2, 3–14.
Rao, K.S., Reddy, M.K., Horning, J.L., Labhasetwar, V., 2008. TAT-conjugated nanoparticles for the CNS delivery of anti-HIV drugs. Biomaterials 29, 4429–4438.
Sarko, D., Beijer, B., Garcia, B.R., Nothelfer, E.M., Leotta, K., Eisenhut, M., Altmann, A., Haberkorn, U., Mier, W., 2010. The pharmacokinetics of cell-penetrating peptides. Mol. Pharm. 7, 2224–2231.
Scott, A.J., Woods, J.P., 2000. Monitoring internalization of Histoplasma capsulatum by mammalian cell lines using a fluorometric microplate assay. Med. Mycol. 38, 15–22.
Suk, J.S., Suh, J., Choy, K., Lai, S.K., Fu, J., Hanes, J., 2006. Gene delivery to differentiated neurotypic cells with RGD and HIV Tat peptide functionalized polymeric nanoparticles. Biomaterials 27, 5143–5150.
Tobio, M., Gref, R., Sanchez, A., Langer, R., Alonso, M.J., 1998. Stealth PLA–PEG nanoparticles as protein carriers for nasal administration. Pharm. Res. 15, 270–275.
Vercauteren, D., Vandenbroucke, R.E., Jones, A.T., Rejman, J., Demeester, J., De Smedt, S.C., Sanders, N.N., Braeckmans, K., 2010. The use of inhibitors to study endocytic pathways of gene carriers: optimization and pitfalls. Mol. Ther. 18, 561–569.
Veronesi, B., 1996. Characterization of the MDCK cell line for screening neurotoxicants. Neurotoxicology 17, 433–443.
Wagner, M.S., McArthur, S.L., Shen, M., Horbett, T.A., Castner, D.G., 2002. Limits of detection for time of flight secondary ion mass spectrometry (ToF-SIMS) and X-ray photoelectron spectroscopy (XPS): detection of low amounts of adsorbed protein. J. Biomater. Sci. Polym. Ed. 13, 407–428.
Wang, Q., Rager, J.D., Weinstein, K., Kardos, P.S., Dobson, G.L., Li, J., Hidalgo, I.J., 2005. Evaluation of the MDR–MDCK cell line as a permeability screen for the blood–brain barrier. Int. J. Pharm. 288, 349–359.
Xia, H., Gao, X., Gu, G., Liu, Z., Zeng, N., Hu, Q., Song, Q., Yao, L., Pang, Z., Jiang, X., Chen, J., Chen, H., 2011. Low molecular weight protamine-functionalized nanoparticles for drug delivery to the brain after intranasal administration. Biomaterials 32, 9888–9898.
Yang, H., 2010. Nanoparticle-mediated brain-specific drug delivery, imaging, and diagnosis. Pharm. Res. 27, 1759–1771.

Zegers, M.M., Zaal, K.J., van IJzendoorn, S.C., Klappe, K., Hoekstra, D., 1998. Actin filaments and microtubules are involved in different membrane traffic pathways that transport sphingolipids to the apical surface of polarized HepG2 cells. Mol. Biol. Cell 9, 1939–1949.

Zhang, J.S., Liu, F., Huang, L., 2005. Implications of pharmacokinetic behavior of lipoplex for its inflammatory toxicity. Adv. Drug Deliv. Rev. 57, 689–698.

Zhang, Y., Benet, L.Z., 1998. Characterization of P-glycoprotein mediated transport of K02, a novel vinylsulfone peptidomimetic cysteine protease inhibitor, across MDR1-MDCK and Caco-2 cell monolayers. Pharm. Res. 15, 1520–1524.

Zorko, M., Langel, U., 2005. Cell-penetrating peptides: mechanism and kinetics of cargo delivery. Adv. Drug Deliv. Rev. 57, 529–545.